Optics Letters

Multi-harmonic near-infrared–ultraviolet dual-comb spectrometer

Kristina F. Chang,[1] Daniel M. B. Lesko,[1,2] Carter Mashburn,[1,3] Peter Chang,[1,3] Eugene Tsao,[1,4] Alexander J. Lind,[1,4] and Scott A. Diddams[1,3,4,*]

[1]Time and Frequency Division, National Institute of Standards and Technology, 325 Broadway, Boulder, Colorado 80305, USA
[2]Department of Chemistry, University of Colorado Boulder, Cristol Chemistry and Biochemistry, Boulder, Colorado 80309, USA
[3]Department of Physics, University of Colorado Boulder, Libby Dr., Boulder, Colorado 80302, USA
[4]Department of Electrical, Computer, and Energy Engineering, University of Colorado Boulder, 425 UCB 1B55, Boulder, Colorado 80309, USA
*scott.diddams@colorado.edu

Received 15 December 2023; revised 24 February 2024; accepted 25 February 2024; posted 26 February 2024; published 19 March 2024

Dual-comb spectroscopy in the ultraviolet (UV) and visible would enable broad bandwidth electronic spectroscopy with unprecedented frequency resolution. However, there are significant challenges in generation, detection, and processing of dual-comb data that have restricted its progress in this spectral region. In this work, we leverage robust 1550 nm few-cycle pulses to generate frequency combs in the UV–visible. We combine these combs with a wavelength multiplexed dual-comb spectrometer and simultaneously retrieve 100 MHz comb-mode-resolved spectra over three distinct harmonics at 386, 500, and 760 nm. The experiments highlight the path to continuous dual-comb coverage spanning 200–750 nm, offering extensive access to electronic transitions in atoms, molecules, and solids.

https://doi.org/10.1364/OL.515776

Ultraviolet (UV) and visible spectroscopy of electronic transitions is an essential tool in chemistry, biology, and materials science [1,2]. Grating-based spectrometers are typically used to measure absorption spectra in the UV–visible from 200 to 750 nm (400 to 1500 THz). Broadband measurements are crucial for fully characterizing electronic spectra, which often span hundreds of THz. Conventional spectrometers commonly employ multiple incoherent lamps to cover the UV–visible range (Fig. 1). However, these instruments are generally limited to >100 GHz resolution, hindering accurate spectral analyses required for applications from fundamental spectroscopy to remote sensing [1,3].

Dual-comb spectroscopy (DCS) is an emerging technique with intrinsic advantages in resolution and precision over existing spectroscopy modalities [4–6]. However, DCS in the visible and UV across comparable bandwidths to conventional spectrometers requires (i) the challenging nonlinear generation of frequency combs across multiple harmonic orders [7–9] and (ii) methods for detecting and processing DCS signals over a wide spectral range. Due to inadequate optical powers and challenging phase control, UV DCS itself remains largely unexplored, with only a few recent examples [10–12].

This work addresses these challenges and achieves multi-harmonic DCS in the UV, visible, and near-infrared (NIR) simultaneously, filling a crucial gap in broad bandwidth and high-resolution (100 MHz) UV–visible spectroscopy. We employ intense few-cycle pulses from erbium:fiber (Er:fiber) lasers to generate NIR to UV frequency combs from 380 to 800 nm in a single bulk crystal. The high peak intensities enable the cascaded generation of several bright harmonics, as shown in Fig. 1. A spectral multiplexing DCS setup yields simultaneous multi-octave detection over these harmonics with high signal-to-noise ratio (*SNR*) and comb-mode resolution. The same few-cycle Er:fiber setup has been previously used for high-harmonic generation (HHG) in solids to produce frequency combs spanning the entire UV–visible down to 200 nm [7], illustrating a direct path to DCS with broader bandwidth coverage at shorter wavelengths. In linking few-cycle harmonic generation to multi-wavelength DCS with over 160,000 resolved comb modes at 100 MHz, our work establishes a foundation for spectroscopy with unparalleled resolution over the full UV–visible range to enable the complete mapping of electronic bands in numerous species.

The DCS setup shown in Fig. 2(a) is based on a pair of repetition rate and phase-stabilized Er:fiber frequency combs at 1550 nm (193 THz) and ~100 MHz repetition rate. A description of the stabilization scheme is included in Supplement 1. We employ the amplification and compression procedure of Ref. [15] to generate near transform-limited 20 fs pulses at ~10 nJ/pulse. NIR–UV combs are generated by focusing the few-cycle pulses in a magnesium oxide-doped periodically poled lithium niobate (PPLN) crystal (L = 0.5 mm, Λ = 20.9 μm) with 0.9 TW/cm^2 peak intensities. Supplement 1 includes simulations confirming that $\chi^{(2)}$ processes dominate the mechanism of harmonic generation through Type-0 phase matching. Cascaded $\chi^{(2)}$ generation produces 2ω (760 nm, 395 THz), 3ω (500 nm, 601 THz), and 4ω (386 nm, 776 THz) harmonics in discrete regions of the NIR, visible, and UV, respectively. The harmonic spectrum is plotted in Fig. 1, and an image of the spectrally dispersed harmonics is shown in Fig. 2(a).

Improvements in spectral overlap between the pair of combs lead to favorable increases in the *SNR* of DCS. In the optical

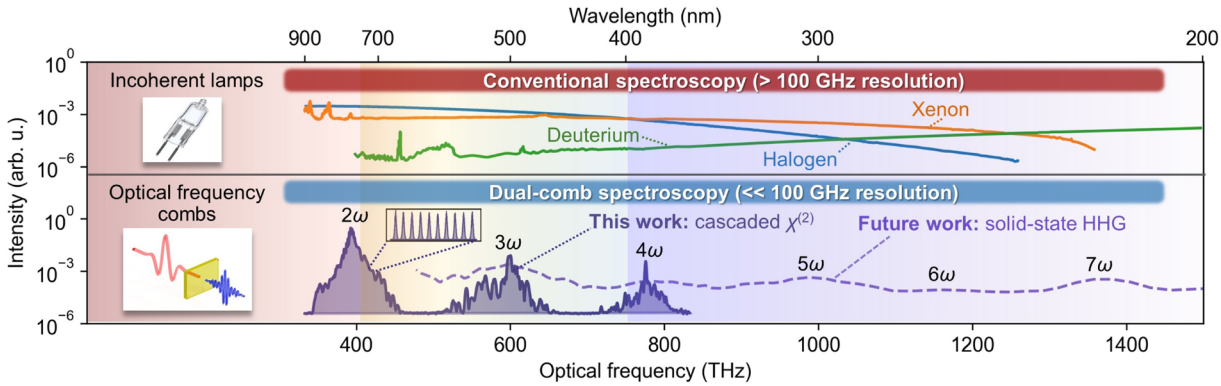

Fig. 1. Light sources for spectroscopy in the UV (750–1500 THz), visible (400–750 THz), and NIR (<400 THz), shaded in red, orange–blue, and purple, respectively. Lamp spectra (blue, orange, green curves) are adapted from Ref. [2]. A NIR–UV frequency comb (solid purple curve) is generated by perturbative $\chi(2)$ harmonic generation in periodically poled lithium niobate (PPLN) with few-cycle pulses. The few-cycle setup also extends to non-perturbative high-harmonic generation (HHG) in zinc oxide [7], providing complete UV–visible coverage (dashed purple curve). The relative scaling of the comb spectra reflects their intensities.

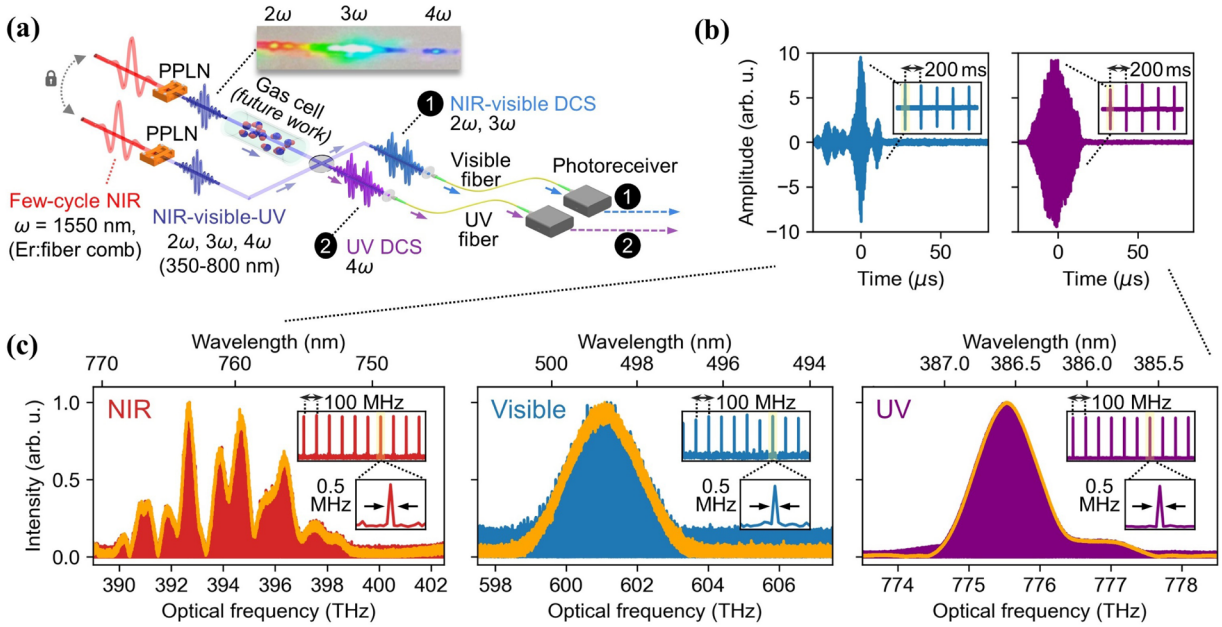

Fig. 2. NIR–UV dual-comb spectrometer and results. (a) Multi-harmonic spectrometer setup. (b) Interferogram streams obtained from visible–NIR (blue curve) and UV (purple curve) dual-comb channels. (c) Comb-mode-resolved spectra in the NIR (red plot), visible (blue plot), and UV (purple plot) obtained from 20 s interferogram streams. The orange traces are dual-comb spectra resulting from a coherent average of 500 self-corrected interferograms over a 100 s measurement time.

setup, the center frequency and structure of each harmonic can be tuned by adjusting the position of the PPLN in the focus of the beam and the spectrum of the few-cycle pulse. Ultimately, experimental parameters are tuned to maximize the spectral overlap of the 4ω UV harmonics of each comb at the sacrifice of optimal spectral overlap at the 2ω NIR and 3ω visible harmonics. A comparison of the two comb spectra and the optical powers of each harmonic is included in Supplement 1.

As shown in Fig. 2(a), NIR–UV DCS is performed by heterodyning two combs that are combined using a 50/50 beam splitter. DCS detection employs a wavelength-multiplexed setup with distinct channels for different wavelength ranges. The beam splitter generates parallel channels focused into visible and UV single-mode fibers, creating dedicated NIR–visible and UV DCS channels. Subsequently, streams of NIR–visible and UV DCS interferograms are simultaneously measured through fast silicon photodetectors and digitized at 100 MHz using a high-speed 16-bit analog-to-digital card.

The combination of single-mode fibers and the wavelength-multiplexed detection scheme provides several advantages. Firstly, the use of a single-mode fiber enhances DCS *SNR* by ensuring high-quality spatial mode overlap between heterodyning combs. We have observed that this increases the signal-to-noise ratios of our DCS measurements by a factor of ~5. Secondly, exploiting the chromatic focal shift from the aspheric lens enables flexible tuning of frequency coupling efficiency by adjusting the distance from the lens to the fiber entrance. This selective frequency coupling facilitates the

removal of the residual fundamental laser ω and ensures specific coupling of 2ω–3ω into the NIR–visible DCS channel and 4ω into the UV DCS channel. Additionally, varying the distance between the aspheric lens and the entrance of the visible single-mode fiber tunes the coupling efficiency and transmission of 2ω and 3ω. This allows the transmitted power of the 2ω harmonic to be attenuated relative to the 3ω harmonic and reduces the risk of detector saturation with the bright 2ω harmonic. Finally, the multiplexing scheme enabled by single-mode fiber coupling allows for parallel acquisition on separate detectors. Since the experimental *SNR* is expected to decrease with increasing optical bandwidth (see Supplement 1), the use of multiple detectors is anticipated to increase the *SNR* by reducing the bandwidth on each detector [4,16].

Figure 2(b) shows a continuous stream of recorded interferograms from NIR–visible and UV DCS. To prevent aliasing in both channels, a small repetition rate difference Δf_r of 5 Hz is used, corresponding to sampling in the first Nyquist window and resulting in an interferogram spacing of $1/\Delta f_r$ = 200 ms in the time domain. Continuous streams of interferograms are recorded for 100 s (500 interferograms) and subsequently post-processed to correct for phase and repetition rate drifts using a self-correction algorithm [17,18]. Finally, we note that UV DCS interferograms were also collected at Δf_r = 171 Hz, the largest repetition rate difference that could be adopted without aliasing, but resulted in no substantial difference in *SNR* for the same measurement time.

Spectra demonstrating NIR–UV DCS at the 2ω to 4ω harmonics are plotted in Fig. 2(c). The spectra result from a Fourier transform of 500 coherently averaged interferograms and a 20 s, 100 interferogram stream. Zooming into the center of the DCS spectra from 20 s streams reveals individual comb beatnotes spaced by the 100 MHz laser repetition rate. The beatnotes are transform-limited (<0.5 MHz optical width, <25 mHz radio frequency width), illustrating the combined effectiveness of comb stabilization and post-processing for comb-mode resolution. In addition, this demonstration confirms that the mutual coherence of the combs is maintained after multiple nonlinear processes including few-cycle pulse generation and cascaded harmonic generation at high peak intensities.

Table 1 summarizes dual-comb bandwidths and frequency domain *SNR* for a 100 s measurement. The reduction in DCS bandwidth at higher frequencies aligns with the decreased bandwidth observed for higher multiplicity harmonic orders, as illustrated in Fig. 1. Notably, the *SNR* in the UV surpasses that in the NIR–visible. The disparity is attributed to the broader bandwidth of the NIR–visible channel measured on a single detector [16], reducing its *SNR*. Additionally, a spectral shape mismatch between the two combs in the NIR–visible contributes to diminished *SNR* in this region (see Supplement 1). In the future, the *SNR* in the NIR and visible can be enhanced by measuring

Table 1. Dual-Comb Spectrometer Performance[a]

Harmonic	Bandwidth	SNR	Quality Factor
2ω (NIR)	9 THz	259	$2.3 \times 10^6\sqrt{\text{Hz}}$
3ω (visible)	4 THz	117	$4.7 \times 10^5\sqrt{\text{Hz}}$
4ω (UV)	3 THz	757	$2.3 \times 10^6\sqrt{\text{Hz}}$

[a]Bandwidth values derived from the full spectral range above the noise floor in each wavelength region. *SNR* values represent frequency domain signal-to-noise ratios for a 100 s measurement.

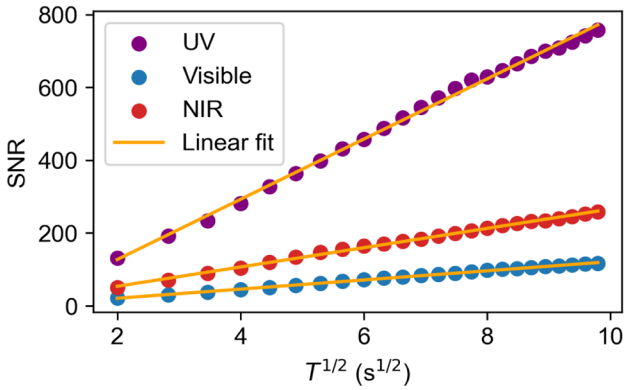

Fig. 3. Frequency domain signal-to-noise ratio (*SNR*) as a function of the square root of the measurement time ($T^{1/2}$).

NIR and visible DCS on separate detectors. Nevertheless, *SNR* levels exceeding 100 for a 100 s measurement are comparable or greater than those recently achieved by UV and visible DCS [8,10,11] and suggest that the spectrometer is suited for simultaneous NIR–UV DCS on gas samples.

In Fig. 3, we illustrate the frequency domain *SNR* scaling with the square root of the measurement time $T^{1/2}$ up to T = 100 s. Linear fits in each spectral regions yield $R^2 > 0.99$. These results confirm the linear scaling of *SNR* with $T^{1/2}$, affirming the preservation of mutual coherence between the two combs over T = 100 s [4,16]. The continued linearity of *SNR* scaling up to 100 s also implies that longer measurement times could enable even higher *SNR*.

Figure 4 provides an overview of all known visible and UV DCS demonstrations to date. In Fig. 4(a), we compare the spectral resolutions and frequency ranges achieved in previous studies with those in this work. Six studies, including three in the UV [10–12] and three in the visible [8,14], are considered. Among these, only one conducted DCS over a multi-wavelength range, though not simultaneously [8]. Specifically, Ref. [8] demonstrated 108.4 MHz comb-mode-resolved DCS in the mid-infrared (MIR), NIR, and visible using discrete harmonics from 450 to 3750 nm generated in a PPLN waveguide with a MIR pump. While a UV harmonic at 395 nm was generated, its power was insufficient for spectroscopy. In contrast, this work showcases DCS at shorter wavelengths by leveraging the generation of optically bright UV harmonics, enabling simultaneous access to the UV and visible with 100 MHz resolution. Notably, among the three previous UV DCS demonstrations [10–12], one achieved comb-mode resolution at 500 MHz over less than 1 THz of bandwidth. Here, we measure 16 THz of simultaneously resolved bandwidth, corresponding to 160,000 individually resolved comb modes.

Figure 4(b) compares the quality factors of DCS examples for which estimates were possible. Quality factors are a metric for comparing the performance of spectrometers and are defined in analogy to the commonly used DCS figure of merit [1,4,11]: $SNR \times M / T^{1/2}$. *SNR* is the frequency domain signal-to-noise ratio, and $M = \Delta\omega/\omega_{res}$, where $\Delta\omega$ is the spectral bandwidth, ω_{res} is the resolution, and T is the measurement time. Values used to calculate quality factors are summarized in Table 1. The quality factors fall between 4×10^5 and 3×10^6 in each spectral region, approaching those of more established MIR and NIR DCS experiments from 10^6-$10^7\sqrt{\text{Hz}}$ [4,19–21]. The quality

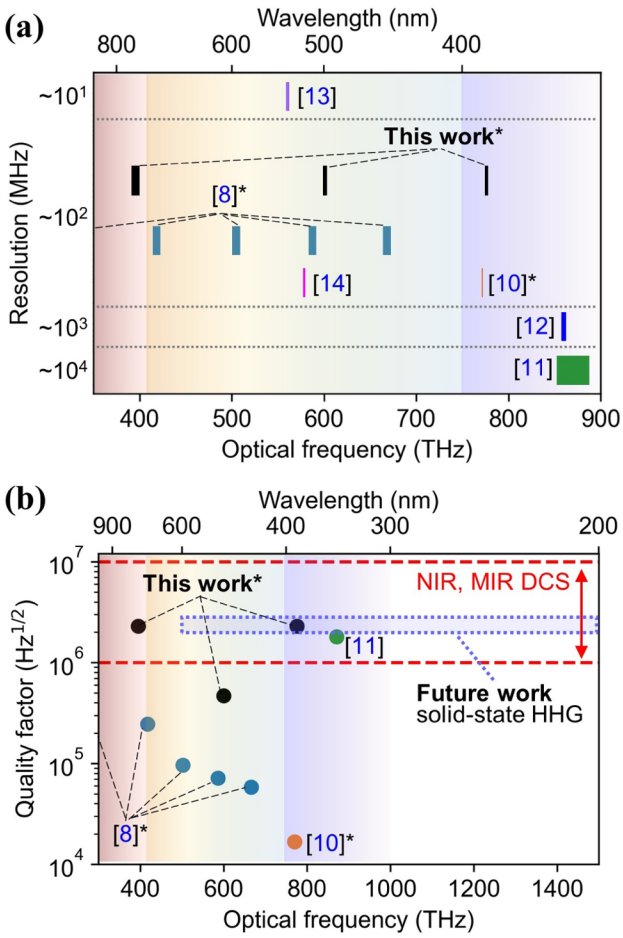

Fig. 4. Literature comparisons. (a) Overview of resolution and (b) quality factors for UV and visible dual-comb studies [8,10–14]. UV, visible, and NIR regions are shaded in red, orange–blue, and purple, respectively. Typical MIR and NIR dual-comb quality factor ranges are denoted in red. A quality factor estimate for future dual-comb from 200 to 600 nm [7] is shown in a dashed purple box. * indicates comb-mode resolved studies.

factors of this visible and UV DCS experiments exceed those of recent experiments in the same spectral range [8,10,11].

Here, DCS at discrete UV–visible harmonics from PPLN is enabled by few-cycle Er:fiber laser. As previously shown, this laser also provides continuous, shorter-wavelength UV–visible combs, albeit at lower powers, when applied to high-harmonic generation (HHG) in a solid (Fig. 1) [7]. Whereas PPLN harmonic generation is limited to >330 nm due to the low transparency of PPLN in the UV [9], HHG generates 2ω through 7ω harmonics, extending the UV coverage to 200 nm, which could enable deep-UV DCS for the first time. A predicted quality factor of $2.5 \times 10^6\sqrt{\text{Hz}}$ over the 200–600 nm span of the comb (see Supplement 1) is shown in Fig. 4(b). This quality factor is equivalent to the results of this work and recent UV and visible DCS studies, indicating the potential of HHG combs for future UV–visible DCS.

In summary, this work demonstrates a DCS spectrometer with simultaneous multi-wavelength coverage from NIR–UV and with high-quality factors and *SNR*. To the best of our knowledge, this is the first DCS demonstration to access both the visible and UV regions. A future extension of the optical setup presented in this work to few-cycle HHG should enable high-resolution, 100 MHz spectroscopy across the entire UV–visible for the first time, representing a key advance in instrumentation for both fundamental and applied spectroscopy.

Funding. National Institute of Standards and Technology (70NANB 18H006); U.S. Air Force (FA9550-16-1-0016, FA9550-22-1-0483).

Acknowledgment. The authors thank J. Genest, M. Walsh, E. Baumann, R. Cole, I. Coddington, and D. Slichter for valuable discussions and feedback. K.F. Chang acknowledges the National Research Council Research Associate Programs Fellowship for funding. E.J. Tsao acknowledges the National Defense Science and Engineering Graduate Fellowship for funding.

Disclosures. The authors declare no conflicts of interest.

Data availability. Data in this paper may be obtained from the authors upon reasonable request.

Supplemental document. See Supplement 1 for supporting content.

REFERENCES

1. S. Galtier, P. Clément, and P. Rairoux, Remote Sens. **12**, 3444 (2020).
2. A. Das, *Portable UV–Visible Spectroscopy - Instrumentation, Technology, and Applications* (John Wiley & Sons, Ltd., 2021), pp. 179–207.
3. V. Schuster, C. Liu, R. Klas, *et al.*, Opt. Express **29**, 21859 (2021).
4. I. Coddington, N. Newbury, and W. Swann, Optica **3**, 414 (2016).
5. M. L. Weichman, P. B. Changala, J. Ye, *et al.*, J. Mol. Spectrosc. **355**, 66 (2019).
6. N. Picque and T. Hansch, Nat. Photonics **13**, 146 (2019).
7. D. Lesko, K. Chang, and S. Diddams, Optica **9**, 1156 (2022).
8. Y. Di, Z. Zuo, D. Peng, *et al.*, Photonics Res. **11**, 1373 (2023).
9. T.-H. Wu, L. Ledezma, C. Fredrick, *et al.*, Nat. Photonics **1**, 1 (2024).
10. B. Xu, Z. Chen, T. W. Hänsch, *et al.*, Nature **627** 289 (2024).
11. B. Bernhardt, L. Furst, A. Kirchner, *et al.*, "Broadband near-ultraviolet dual comb spectroscopy," Research Square, rs.3.rs-2760097 (2023).
12. Y. Zhang, J. J. McCauley, and R. J. Jones, *CLEO 2023* (2023), paper SF3F.6.
13. Y. Sugiyama, T. Kashimura, K. Kashimoto, *et al.*, Sci. Rep. **13**, 2549 (2023).
14. T. Ideguchi, A. Poisson, G. Guelachvili, *et al.*, Opt. Lett. **37**, 4847 (2012).
15. D. Lesko, H. Timmers, S. Xing, *et al.*, Nat. Photonics **15**, 281 (2021).
16. N. R. Newbury, I. Coddington, and W. Swann, Opt. Express **18**, 7929 (2010).
17. N. B. Hébert, J. Genest, J.-D. Deschênes, *et al.*, Opt. Express **25**, 8168 (2017).
18. H. Yu, K. Ni, Q. Zhou, *et al.*, Opt. Express **27**, 29425 (2019).
19. A. M. Zolot, F. R. Giorgetta, E. Baumann, *et al.*, Opt. Lett. **37**, 638 (2012).
20. A. J. Lind, A. Kowligy, H. Timmers, *et al.*, Phys. Rev. Lett. **124**, 133904 (2020).
21. M. Liu, R. M. Gray, L. Costa, *et al.*, Nat. Commun. **14**, 1044 (2023).